Ghosh, A., Thyagarajulu, G., Steinberger, B. (2017): The Importance of Upper Mantle Heterogeneity in Generating the Indian Ocean Geoid Low. - *Geophysical Research Letters*, *44*, 19, pp. 9707—9715.

DOI: http://doi.org/10.1002/2017GL075392

AGU PUBLICATIONS

Geophysical Research Letters

RESEARCH LETTER
10.1002/2017GL075392

Key Points:
- The current study successfully explains the occurrence of the Indian Ocean Geoid low using a global convection model driven by present-day density anomalies derived from tomography
- Upper to middle mantle low-density anomalies are mainly responsible for the formation of this low
- The recent tomography models have the necessary resolution to reproduce this geoid low

Supporting Information:
- Supporting Information S1

Correspondence to:
A. Ghosh,
aghosh@ceas.iisc.ernet.in

Citation:
Ghosh A., Thyagarajulu, G., & Steinberger, B. (2017). The importance of upper mantle heterogeneity in generating the Indian Ocean geoid low. *Geophysical Research Letters*, *44*, 9707–9715. https://doi.org/10.1002/2017GL075392

Received 29 AUG 2017
Accepted 25 SEP 2017
Accepted article online 13 OCT 2017
Published online 14 OCT 2017

The Importance of Upper Mantle Heterogeneity in Generating the Indian Ocean Geoid Low

Attreyee Ghosh[1], G. Thyagarajulu[1], and Bernhard Steinberger[2]

[1]Centre for Earth Sciences, Indian Institute of Science, Bangalore, India, [2]Helmholtz Centre Potsdam, GFZ German Research Centre for Geosciences, Potsdam, Germany

Abstract One of the most pronounced geoid lows on Earth lies in the Indian Ocean just south of the Indian peninsula. Several theories have been proposed to explain this geoid low, most of which invoke past subduction. Some recent studies have also argued that high-velocity anomalies in the lower mantle coupled with low-velocity anomalies in the upper mantle are responsible for these negative geoid anomalies. However, there is no general consensus regarding the source of this particular anomaly. We investigate the source of this geoid low by using models of density-driven mantle convection. Our study is the first to successfully explain the occurrence of this anomaly using a global convection model driven by present-day density anomalies derived from tomography. We test various tomography models in our flow calculations with different radial and lateral viscosity variations. Some of them produce a fairly high correlation to the global geoid, but only a few (SMEAN2, GyPSuM, SEMUCB, and LLNL-JPS) could match the precise location and pattern of the geoid low in the Indian Ocean. The source of this low stems from a low-density anomaly stretching from a depth of 300 km down to ~900 km in the northern Indian Ocean region. This density anomaly potentially originates from material rising along the edge of the African Large Low Shear Velocity Province and moving toward the northeast, facilitated by the movement of the Indian plate in the same direction.

Plain Language Summary One of the lowest geoid anomalies on Earth lies in the Indian Ocean just south of the Indian peninsula. Several theories have been proposed to explain this gravity low. Most of these theories try to explain the existence of this anomaly with the help of cold, dense oceanic plate that sank into the mantle in the past and which could potentially be present below the Indian Ocean at depths greater than 1,000 km. However, there is no general consensus regarding the source of this particular negative geoid anomaly. We investigate the source of this low by using models of density-driven mantle convection. Our study finds that the source of this low stems from a low-density anomaly stretching from a depth of 300 km down to ~900 km in the northern Indian Ocean region. This density anomaly potentially originates from hot buoyant material rising from deep mantle beneath Africa and moving toward the northeast, facilitated by the movement of the Indian plate in the same direction. Our study is the first to successfully explain the occurrence of this geoid low using present-day density anomalies.

1. Introduction

Long wavelength geoid anomalies have their origin in the Earth's mantle. They provide important information regarding the density and viscosity structure of the Earth's interior. These long wavelength geoid variations have been successfully replicated by numerous models of mantle convection (Cadek & Fleitout, 2003; Ghosh et al., 2010; Hager et al., 1985; Hager & Richards, 1989; Moucha et al., 2007; Steinberger, 2000; Wen & Anderson, 1997; Yoshida & Nakakuki, 2009; Zhong, 2001; Zhong & Davies, 1999). The convective flow in these models is generated by density anomalies that are derived from tomography and/or geodynamic models. However, there are certain features of the global geoid that could not be accurately reproduced by the mantle convection models. One such feature is the negative geoid anomaly situated in the Indian Ocean directly south of the Indian peninsula. It is the most negative geoid anomaly on Earth when the geoid is defined relative to the reference ellipsoid. Most of the geoid lows have been linked to past subduction (Chase & Sprowl, 1983; Hager & Richards, 1989; Richards & Engebretson, 1992; Steinberger, 2000) as well as subduction coupled with mantle upwellings (Spasojevic et al., 2010). Several theories have been put forward to explain this negative anomaly,

such as depression of the core-mantle boundary (Negi et al., 1987), isostatically uncompensated crust (Ihnen & Whitcomb, 1983), and presence of paleo back-arc basins in the Neo-Tethys Ocean prior to India's collision with Eurasia (Nerlich et al., 2016). A recent study by Reiss et al. (2017) found a hot midmantle anomaly beneath the Indian Ocean geoid low (IOGL) and concluded that this high-temperature anomaly along with cold material below 660 km farther south could be responsible for the geoid low.

We investigate the source of this anomaly by using instantaneous models of density-driven mantle convection with the code CitcomS (Zhong et al., 2000). We test various tomography models in our flow calculations with different radial and lateral viscosity variations. In particular, we examine whether recent tomography models can accurately reproduce the localized anomaly in the region rather than just the longest wavelength components. Moreover, the role of lateral viscosity variations in influencing the geoid is controversial (Ghosh et al., 2010; Moucha et al., 2007; Tosi et al., 2009; Yoshida & Nakakuki, 2009; Zhong & Davies, 1999). We also address if the Indian Ocean geoid anomaly is affected by these lateral variations in viscosity.

2. Methods

We use the three-dimensional viscous finite element parallel convection code CitcomS to calculate gravitational potential from large-scale mantle convection. We solve the Stokes flow equations, on an average horizontal grid size of $0.6 \times 0.6°$, given a density and rheology distribution in spherical coordinates Zhong et al. (2008). Seismic velocity anomalies are converted to density anomalies, which drive flow in the mantle. We use a constant velocity-density scaling ($d\ln\rho/d\ln V_s$) of 0.25 for the *S* wave models and 0.5 ($d\ln\rho/d\ln V_p$) for the *P* wave models throughout the mantle. Various studies have examined the dependence of seismic velocities on density in the mantle, and several of them have argued for a nonlinear relation between them (cf. Cammarano et al., 2003; Forte et al., 2015; Moulik & Ekstrom, 2016). We have tested a few cases where we use depth-dependent scalings (Model 2 of Steinberger and Calderwood (2006) with scaling reduced by a factor 2 in the uppermost 220 km; preferred scaling used by Cadek and Fleitout (1999)) and a radial viscosity structure to compute the geoid. The constant and the depth-dependent scalings yield very similar results in the IOGL region, and hence, these results are not shown and we restrict our discussion to the constant scaling cases. Positive density anomalies in the top 300 km below cratons (based on 3SMAC by Nataf and Ricard, 1996) are set to zero in some cases, although they seem to have a minor effect on the predicted geoid. The geoid is calculated up to a maximum spherical harmonic degree 63 including effects of self-gravitation. The actual degree of expansion may be lower depending on the tomography model used. The predicted geoid anomaly results from a combination of internal density anomalies as well as dynamic topography at the surface and at the core-mantle boundary (CMB) (Adam et al., 2014; Hager, 1984). The computed geoid is correlated with the observed geoid from Chambat et al. (2010), which is relative to the hydrostatic equilibrium shape (and not the reference ellipsoid). We also compute regional correlation as well as regional RMS amplitude and RMS misfit in the IOGL region. Although the emphasis of this study is to reproduce the IOGL and thereby explain its origin, we think it is imperative that our output geoid matches the observed geoid globally as well. We use several tomography models: TX2008 (Simmons et al., 2007), S40RTS (Ritsema et al., 2011), SAW642AN (Megnin & Romanowicz, 2000), SEMUCB-WM1 (French & Romanowicz, 2014), GyPSuM (Simmons et al., 2010), SAVANI (Auer et al., 2014), SMEAN2 (a composite mantle tomography model composed of S40RTS, GyPSuM-S, and SAVANI generated using the approach of Becker and Boschi (2002)), and the recent LLNL-G3D-JPS model (Simmons et al., 2015). The first four are *S* wave models, whereas GyPSuM and LLNL have both *P* and *S* wave versions. GyPSuM was developed by simultaneous inversion of body wave travel times and geodynamic observations.

We use both radial and lateral viscosity variations for computing the geoid. We follow the methodology adopted in Ghosh et al. (2010) and use a five layer radial viscosity structure divided into lithosphere (0–100 km), asthenosphere (100–300 km), upper mantle (UM) (300–410 km), transition zone (410–660 km), and lower mantle (LM) (660 km CMB) in some cases. In others, we use the SH08 viscosity structure, which is derived in the same way as Model C of Steinberger and Holme (2008), but with the additional requirement that the lowest viscosity occurs in the upper mantle, not the transition zone (see Figure 1 of Wang et al., 2015). Moreover, we tested a case where there is a viscosity jump between 800 and 1,200 km as suggested by Rudolph et al. (2015), which did not produce a good fit to the observed geoid. Out of all viscosity structures that we tested, the SH08 structure, which has been shown earlier to predict geoid and deviatoric stresses that yield a good fit to observations (Wang et al., 2015), provides the closest match with the observed geoid. The 5

layer viscosity structures either predict an additional geoid trough near Australia or a much elongated trough (Figure S1 in the supporting information). They also over predict the amplitude of the IOGL.

We add lateral viscosity variations on top of these radial viscosity structures. The lateral variations are added in two ways. One way is by introducing temperature-dependent viscosity whereby viscosities are allowed to vary with temperatures as $\eta = \eta_0 \cdot \exp(E(T_0 - T))$. T_0, T and $T' = T - T_0$ are the nondimensionalized reference, actual, and residual temperatures and E controls how strong is the temperature dependence. We use a thermal expansivity of $3 \times 10^{-5} K^{-1}$ to convert relative density anomalies to residual temperature and nondimensionalize it by dividing with a scaling temperature of 1,300 K (e.g., Ghosh et al., 2010, 2013). We test E values of 5 and 10 that lead to 2 and 4 orders of magnitude variations in viscosity as a function of T. The second way is to specify specific viscosity values to certain tectonic regions. Plate boundaries are assigned a viscosity 10 times lower than the intraplate regions to denote their "weakness," while the cratonic interiors (based on 3SMAC cratons) are designated viscosity values an order of magnitude higher than the intraplate regions, both down to a depth of 100 km. The models are calculated with free slip boundary conditions both at the surface and the core-mantle boundary.

3. Results

The output geoid from the tomography models S40RTS, TX2008, and SAW642AN, using the SH08 viscosity structure, yield a considerably high correlation to the observed geoid globally (Figures 1 and S2). However, when it comes to the geoid low in the Indian Ocean, none of these models are able to match its location as well as its pattern. S40RTS predicts a low that is far south of the actual location of the IOGL, whereas SAW642AN does not produce any significant low in that region. TX2008, on the other hand, predicts a linear negative anomaly that stretches up to the western edge of Australia. In contrast, the geoid predicted by SEMUCB-WM1 matches the observed geoid better with a global and regional correlation of 0.87 and 0.69, although the predicted low is more elongated in shape as compared to the observed (Figure 1). SMEAN2 also yields a high global and regional correlation, although the fit to the observed geoid is more likely to stem from GyPSuM-S, which is one of its components, as neither S40RTS nor SAVANI fits the regional geoid low well. GyPSuM-P predicts a global and regional geoid that fit the observed geoid quite well. The match to the global geoid by the GyPSuM S wave model is even higher with a correlation of 0.89. The regional geoid from this model also matches the IOGL considerably well although the signal is more elongated than what is observed. The geoid predicted from the LLNL-G3D-JPS P and S wave models do not yield as high a correlation to the observed geoid globally as the other models. The regional fit is quite good visually although the correlation coefficient is not high (0.68). This is because the drop in correlation happens mostly in the regions surrounding the IOGL (primarily west of the Indian Ocean ridge). The geoid from all the above models slightly overpredict the amplitude of the IOGL except for SEMUCB which predicts a geoid whose RMS amplitude closely matches that of the observed geoid in the Indian Ocean region. Removing lateral viscosity variations does not change the pattern considerably but somewhat decreases global and regional correlation for all the models except LLNL-JPS. Of all the tomography models, GyPSuM-P yields the highest correlation to the IOGL, which is perhaps not surprising as it is developed by simultaneous inversion of body wave travel times and geodynamic observations, the geoid being one of them. The above results indicate that the more recent tomography models have the right ingredients that can closely reproduce the geoid low in the Indian Ocean. We also test the effect of temperature-dependent viscosities on the geoid. For the global geoid, turning on temperature dependence hardly makes a difference. For the regional geoid, a strong temperature dependence of viscosity ($E = 10$) slightly worsens the fit (Figure S3) except for the LLNL model which undergoes a moderate improvement in fit. A moderate temperature dependence ($E = 5$) hardly affects the IOGL except for LLNL, which improves slightly. Here we choose to mainly show the results from the models that incorporate lateral viscosity variations within the lithosphere only that stem from stiff cratons (10 times stronger) and weak plate boundaries (10 times weaker) compared to the intraplate regions.

Based on the geoid kernels that take into account contributions from both driving density anomaly as well as boundary deformation in an incompressible Newtonian fluid, a geoid low would be produced by either a positive density anomaly in the lower mantle below ~1,000 km or a negative density anomaly above ~1,000 km (Hager, 1984; Hager et al., 1985). The nondimensionalized residual temperature anomalies T' along three profiles AA′, BB′, and CC′ show broad high-temperature anomalies in the vicinity of the IOGL in the upper mantle that extend into the lower mantle in all the models down to about 800 km (Figure 2). These temperature anomalies correspond to density anomalies and are analogous to velocity anomalies in tomography models

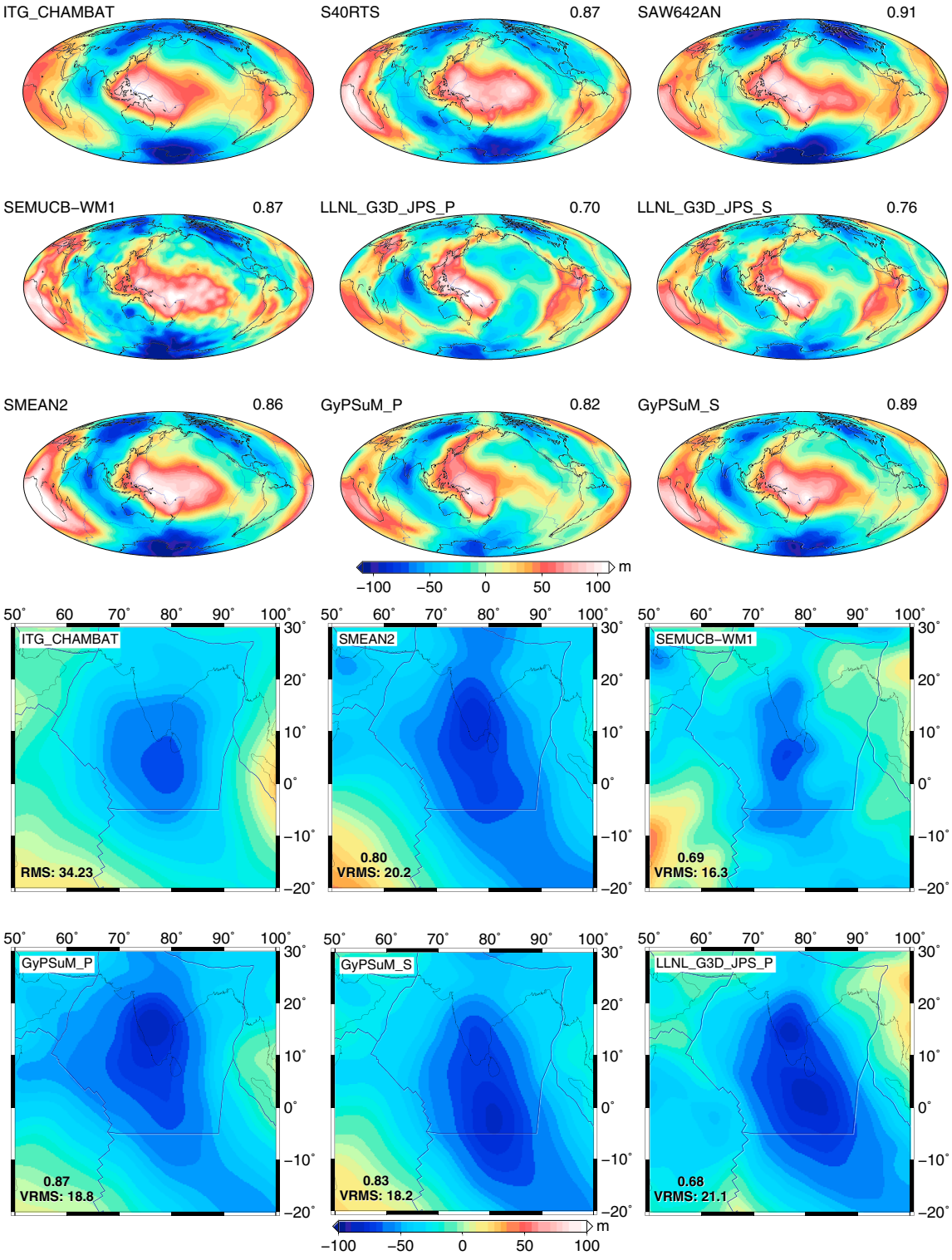

Figure 1. Observed geoid from Chambat et al. (2010) and predicted geoid from different tomography models using SH08 viscosity structure with lateral variations due to strong cratons and weak plate boundaries in the top 100 km. The correlation coefficients with the observed geoid are given on the top right of each figure. For the bottom row, the regional correlation coefficients are noted along with VRMS in meters, which indicates the regional RMS misfit with the observed geoid.

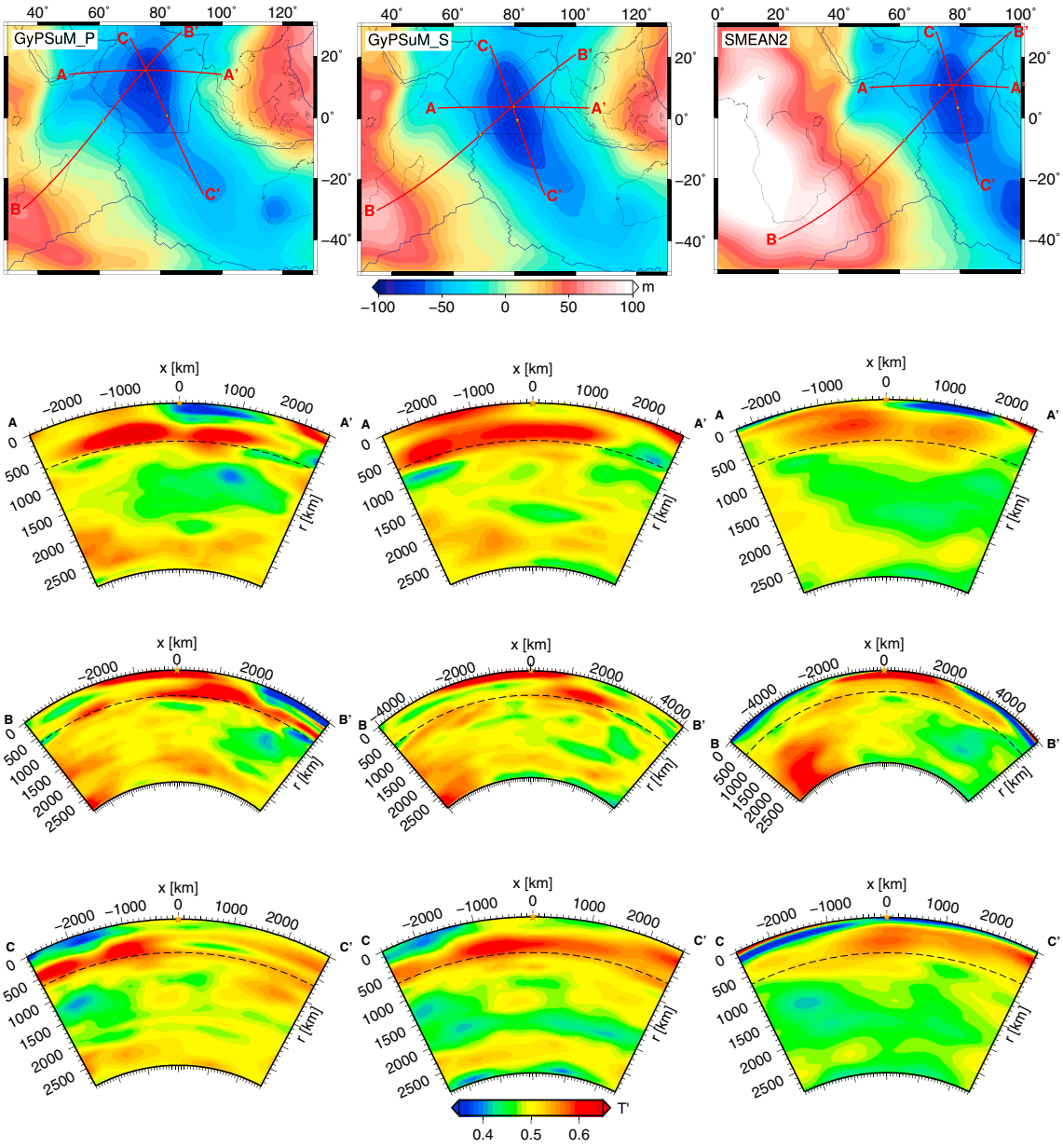

Figure 2. Nondimensionalized residual temperature (T') along three profiles in the Indian Ocean geoid low region for GyPSuM-P, GyPSuM-S, and SMEAN2 tomography models.

with the reference being 0.5 instead of 0. Farther down into the mantle, the positive temperature anomaly is replaced by a neutral or a slightly negative temperature anomaly, whose amplitude is much lower than what would be expected of a cold dense slab. So the source of the geoid low seems to stem from a low-density material in the upper to midmantle, rather than dense lower mantle slabs, as has been proposed by some previous studies (Nerlich et al., 2016; Rao & Kumar, 2014).

In order to investigate the role of the bottom ~2,000 km of the mantle in producing the geoid low, we experiment with cases where we include the density anomalies from the top ~1,000 km only for the models SEMUCB, SMEAN2, LLNL-G3D-JPS, and GyPSuM. As one would expect, the global fit to the geoid decreases significantly for all the models when the lower 2,000 km of the mantle is stripped off any density anomalies, as does the fit to the IOGL (Figures 3 and S4). Several studies have argued about the importance of high-velocity anomalies in the lower mantle in affecting the geoid low (Nerlich et al., 2016; Spasojevic et al., 2010; Rao & Kumar, 2014). So we consider two further cases, one where the full tomography in the top 1,000 km is included whereas

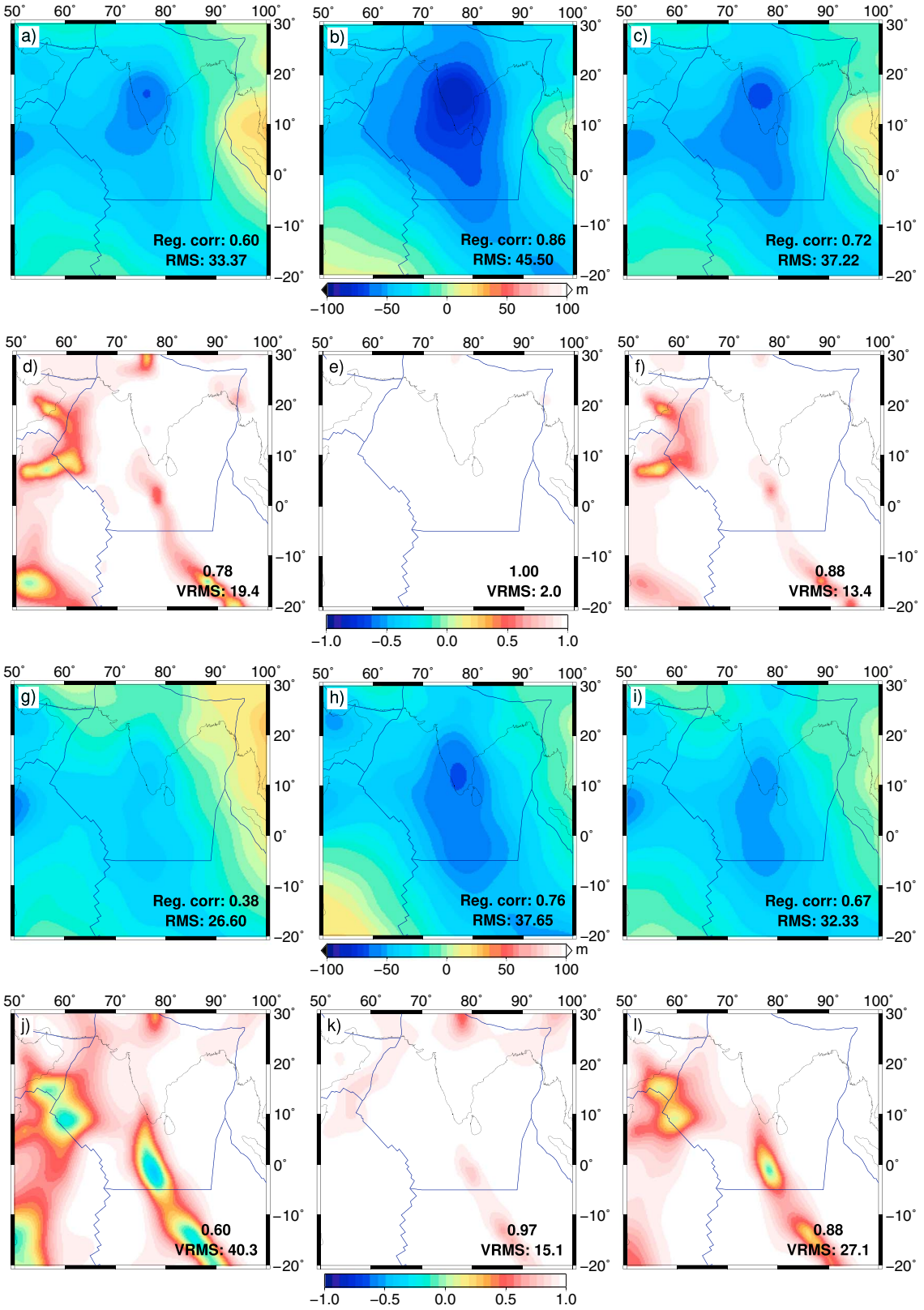

Figure 3. Geoid predicted from GyPSuM-P (a-c) and SMEAN2 (g-i) by including density anomalies in the mantle up to ~1,000 km and (a and g) no density anomalies below that, (b and h) only low-density anomalies below that, (c and i) only high-density anomalies below that. Regional correlation coefficients with the observed geoid are noted within the figures. (d–f) Local correlation, computed by moving a 50 km radius cap across the domain, between the geoid predicted by full GypSuM-P and that predicted by Figures 3a–3c, respectively. (j–l) Same as Figures 3d–3f but for SMEAN2.

below that depth we consider only the high-velocity anomalies. The global correlation increases for all the tomography models, compared to the case where the entire bottom 2,000 km of mantle was removed. The fit to the IOGL also increases, although it is nowhere close to the case when the entire mantle was involved (Figures 3 and S4). Now we repeat the above experiment, but this time with full tomography in the top 1,000 km and only the low-velocity anomalies included below that. The fit to the IOGL is very close to the case where the entire mantle was included (Figure 3). For GyPSuM-P, there is a perfect correlation between this case and that predicted by full tomography (Figure 3e) and a very low RMS difference. For the other models as well, there is a very high correlation between this case and the case with full tomography (Figure S4). This would indicate that presence of subducted slabs in the lower mantle is not a necessary condition for producing all geoid lows, as has been proposed earlier. On the other hand, the low-density anomalies in the bottom ~2,000 km seem to play a much more important role compared to the high-density slabs. This may seem counterintuitive as low-density anomalies in the lower mantle are supposed to generate geoid highs and not lows. The most likely explanation is that the flow field is affected by the low-density anomalies, such as the large low shear velocity provinces (LLSVPs) outside that region. This is substantiated by the experiment where we remove all tomography below 1,000 km in the IOGL region and retain only the low-velocity anomalies elsewhere with the top 1,000 km having full tomography everywhere. The resultant geoid again shows a very prominent low in the Indian Ocean region and fits the pattern of regional geoid extremely well (Figure S5).

Subducted slabs in the lower mantle may not be adequately represented in tomography models. So we explore the question whether well-defined slabs in the lower mantle could improve the fit to the IOGL. To examine that, we combine the lower mantle slab models stb00d (Steinberger, 2000) or st12den2 (Steinberger et al., 2012) (after removing the low-density anomalies) with the tomography models SEMUCB-WM1, GyPSuM, LLNL-JPS, and SMEAN2 in the upper mantle. We retain the low-velocity anomalies and replace the high-velocity anomalies in the lower mantle of the tomography models with the slabs in the slab models. The resultant geoid yields similar fit to the observed low (0.87 and 0.80 regional correlation for stb00d and st12den2 with GyPSuM-P) as when tomography is included in the entire mantle. This would suggest that having well-defined slabs in the lower part of the mantle has little role to play in forming the negative geoid anomaly in the Indian Ocean.

The reason why high-velocity anomalies in the lower mantle hardly affect the IOGL can be understood from subduction history models: older slabs, which are now in the lower mantle, are most prominent beneath East Asia and its antipode (Steinberger et al., 2017); hence, corresponding geoid lows are predicted in these regions, whereas around the IOGL the corresponding geoid is almost neutral (Figure S6, bottom row).

4. Discussion and Conclusion

Previous mantle flow models had attempted to reproduce the observed geoid on Earth although most of them did not look specifically at the geoid low in the Indian Ocean region. Our study is the first to successfully explain the presence of the IOGL using a global convection model driven by present-day density anomalies derived from tomography. One of the biggest reasons for this success is that the new generation of tomography models are beginning to image more realistic features in the mantle which were absent from earlier models. These newer models have the necessary ingredients to explain the observed geoid height almost everywhere on Earth including in the Indian Ocean region. Our study suggests that the low-density anomalies in the upper to middle mantle below the IOGL in addition to low-density anomalies below 1,000 km depth seem to be responsible for the existence of the negative gravity anomaly in this region. This leads further support to the recent findings by Reiss et al. (2017) which showed the presence of hot material below the IOGL from differential travel time data. The obvious question is, where this low-density anomaly in the upper part of the mantle originates from. No known mantle plume exists in this part of the world. However, when we observe the temperature variations along a vertical profile that extends from the African LLSVP up to the IOGL, we see a high-temperature anomaly arising from the base of the lower mantle, getting deflected eastward and terminating at the base of the low-density anomaly beneath the IOGL (profile BB' in right panel of Figure 2), a feature similar to the one observed by Nerlich et al. (2016) in their mantle model driven by time-dependent subduction. This anomaly reaches the uppermost mantle just beneath La Réunion. The material from that plume, and perhaps other material rising above the African LLSVP, is fed into the low-viscosity asthenosphere and then flows toward the northeast. We speculate that the cause for the tilt and horizontal extent of the plume material could be partly (mainly in the uppermost mantle) due to the fast motion of the Indian plate in northeastern direction, which is modulating the flow direction (cf. Griffiths and Richards, 1989)

and partly (at greater depth) due to the tendency of the base of the plume material to migrate to the center of the LLSVP while the top remains closer to the LLSVP margin as suggested by Steinberger and Torsvik (2012). Time-dependent modeling studies are needed to validate this hypothesis.

The most significant density anomalies inferred from tomography below the IOGL are low-density anomalies in the upper to middle mantle region. The high-density anomalies in the lower mantle are far too weak to give rise to such a strong negative geoid anomaly. Moreover, density anomalies in the lower mantle would not produce such a localized feature as the IOGL; the resultant anomaly would be broader and more diffuse as shown in Figure S6. The geoid predicted using density anomalies in the bottom ~2,000 km only and no tomography above shows two broad positive anomalies over the African and Pacific LLSVPs with two broad diffuse very small amplitude lows sandwiched between them. Only when the upper mantle contribution is added, the resultant geoid low in the Indian Ocean starts taking shape.

Various studies had discussed the origin of geoid lows on Earth. Spasojevic et al. (2010) argued that geoid lows could only be reproduced by high-density slabs in the lower mantle coupled with upwellings in the upper mantle. They suggested that these upwellings were due to buoyant hydrated mantle generated by processes above the subducted slabs. However, they also noted that the IOGL was not matched well by models that could reproduce the other geoid lows. While our study supports their argument of upwelling above 1,000 km depth responsible for the negative geoid anomaly in the Indian Ocean, any high-density anomalies below this upwelling in the tomography models do not significantly contribute to the IOGL (Figures 2 and 3). Moreover, removing high-density anomalies in the lower mantle hardly affect the IOGL (Figures 3 and S4). Nerlich et al. (2016) showed that the presence of double subduction zones in the Neo-Tethys ocean could explain the current geoid observation in the Indian Ocean using plate reconstruction models, in combination with low-density anomalies in the upper part of the mantle that originate from a mantle upwelling. Rao and Kumar (2014) and Rao et al. (2017) also argued for seismic evidence of subducted slabs beneath the IOGL at the lowermost mantle. They suggested lowering of density in the upper mantle due to dehydration of these subducted slabs to be responsible for the geoid low. In this study, we find that the geoid low can in fact be explained by presence of low-density anomalies in the ~300–900 km depth beneath the IOGL, as well as low-density anomalies at greater depth beneath other regions, especially those related to LLSVPs. These suitable density anomalies can be inferred from recent seismic tomography models. High-density anomalies in the lower part of the mantle give a nearly neutral geoid in the IOGL region and therefore only a very minor contribution to the IOGL. The low-density anomalies in the upper mantle below the IOGL seem to be originating from a low-density plume rising at the edge of the African LLSVP (Figure 2, cross section BB′ in right panel). While density anomalies in the lower part of the mantle may contribute to an overall low geoid in that region, its regional-scale geometry can be mostly explained by low-density anomalies in the upper part of the mantle.

Acknowledgments
We would like to thank Nathan Simmons for sharing the LLNL-G3D-JPS tomography model. We would also like to acknowledge IRIS Data Services Products from where most of the other tomography models were downloaded. Convection code CitcomS is hosted at CIG. The models were run at the Supercomputer Education and Research Centre (SERC) at IISc. Figures were prepared using GMT 4.5.12 by P. Wessel and W. F. Smith. The research was funded by ISRO-IISc Space Technology Cell grant STC/P-330. Comments from two anonymous reviewers were helpful in improving the manuscript.

References

Adam, C., Yoshida, M., Suetsugu, D., Fukao, Y., & Cadio, C. (2014). Geodynamic modeling of the South Pacific superswell. *Physics of the Earth and Planetary Interiors*, *229*, 24–39.

Auer, L., Boschi, L., Becker, T. W., Nissen-Meyer, T., & Giardini, D. (2014). Savani: A variable-resolution whole-mantle model of anisotropic shear-velocity variations based on multiple datasets. *Journal of Geophysical Research: Solid Earth*, *119*, 3006–3034. https://doi.org/10.1002/2013JB010773

Becker, T. W., & Boschi, L. (2002). A comparison of tomographic and geodynamic mantle models. *Geochemistry, Geophysics, Geosystems*, *3*, 1003. https://doi.org/2001GC000168

Cadek, O., & Fleitout, L. (1999). A global geoid model with imposed plate velocities and partial layering. *Journal of Geophysical Research*, *104*, 29,055–29,075.

Cadek, O., & Fleitout, L. (2003). Effect of lateral viscosity variations in the top 300 km on the geoid and dynamic topography. *Geophysical Journal International*, *152*, 566–580.

Cammarano, F., Goes, S., Vacher, P., & Giardini, D. (2003). Inferring upper-mantle temperatures from seismic velocities. *Physics of the Earth and Planetary Interiors*, *138*, 197–222.

Chambat, F., Ricard, Y., & Valette, B. (2010). Flattening of the Earth: Further from hydrostaticity than previously estimated. *Geophysical Journal International*, *183*, 727–732.

Chase, C. G., & Sprowl, D. R. (1983). The modern geoid and ancient plate boundaries. *Earth and Planetary Science Letters*, *62*, 314–320.

Forte, A., Simmons, N. A., & Grand, S. P. (2015). Constraints on 3-D seismic models from global geodynamic observables: Implications for the global mantle convective flow, (2nd ed.). In G. Schubert (Ed.), *Treatise of Geophysics* (pp. 805–858). Burlington, MA: Elsevier.

French, S. W., & Romanowicz, B. (2014). Whole-mantle radially anisotropic shear velocity structure from spectral-element waveform tomography. *Geophysical Journal International*, *199*, 1303–1327.

Ghosh, A., Becker, T. W., & Humphreys, E. (2013). Dynamics of the North American continent. *Geophysical Journal International*, *194*, 651–669.

Ghosh, A., Becker, T. W., & Zhong, S. J. (2010). Effect of lateral viscosity variations on the geoid. *Geophysical Research Letters*, *37*, L01301. https://doi.org/10.1029/2009GL040426

Griffiths, R. W., & Richards, M. A. (1989). The adjustment of mantle plumes to changes in plate motion. *Geophysical Research Letters*, *16*, 437–440.
Hager, B. H. (1984). Subducted slabs and the geoid: Constraints on mantle rheology and flow. *Journal of Geophysical Research*, *89*, 6003–6015.
Hager, B. H., Clayton, R. W., Richards, M. A., Comer, R. P., & Dziewonski, A. M. (1985). Lower mantle heterogeneity, dynamic topography and the geoid. *Nature*, *313*, 541–545.
Hager, B. H., & Richards, M. A. (1989). Long-wavelength variations in Earth's geoid: Physical models and dynamic implications. *Philosophical Transactions of the Royal Society of London, Series A: Mathematical, Physical and Engineering Sciences*, *328*, 309–327.
Ihnen, S. M., & Whitcomb, J. H. (1983). The Indian Ocean gravity low: Evidence for an isostatically uncompensated depression in the upper mantle. *Geophysical Research Letters*, *10*, 421–423.
Megnin, C., & Romanowicz, B. (2000). The shear velocity structure of the mantle from the inversion of of body, surface and higher modes waveforms. *Geophysical Journal International*, *143*, 709–728.
Moucha, R., Forte, A., Mitrovica, J., & Daradich, A. D. (2007). Lateral variations in mantle rheology: Implications for convection related surface observables and inferred viscosity models. *Geophysical Journal International*, *169*, 113–135.
Moulik, P., & Ekstrom, G. (2016). The relationships between large-scale variations in shear velocity, density, and compressional velocity in the Earth's mantle. *Journal of Geophysical Research: Solid Earth*, *121*, 2737–2771. https://doi.org/10.1002/2015JB012679
Nataf, H., & Ricard, Y. (1996). 3SMAC: An a priori tomographic model of the upper mantle based on geophysical modeling. *Physics of the Earth and Planetary Interiors*, *95*, 101–122.
Negi, J. G., Thakur, N. K., & Agrawal, P. K. (1987). Can depression of the core–mantle interface causes coincident Magsat and geoidal 'lows' of the central Indian Ocean?. *Physics of the Earth and Planetary Interiors*, *45*, 68–74.
Nerlich, R., Colli, L., Ghelichkhan, S., Schuberth, B., & Bunge, H. P. (2016). Constraining central Neo-Tethys Ocean reconstructions with mantle convection models. *Geophysical Research Letters*, *43*, 9595–9603. https://doi.org/10.1002/2016GL070524
Rao, B. P., & Kumar, M. R. (2014). Seismic evidence for slab graveyards atop the core mantle boundary beneath the Indian Ocean Geoid Low. *Physics of the Earth and Planetary Interiors*, *236*, 52–59.
Rao, B. P. R., Kumar, M. R., & Singh, A. (2017). Anisotropy in the lowermost mantle beneath the Indian Ocean Geoid Low from ScS splitting measurements. *Geochemistry, Geophysics, Geosystems*, *18*, 558–570.
Reiss, A., Thomas, C., Driel, J., & Heyn, B. (2017). A hot midmantle anomaly in the area of the Indian Ocean geoid low. *Geophysical Research Letters*, *44*, 6702–6711. https://doi.org/10.1002/2017GL073440
Richards, M., & Engebretson, D. (1992). Large-scale mantle convection and the history of subduction. *Nature*, *355*, 437–440.
Ritsema, J., Deuss, A., van Heijst, H. J., & Woodhouse, J. H. (2011). S40RTS: A degree-40 shear-velocity model for the mantle from new Rayleigh wave dispersion, teleseismic traveltime and normal-mode splitting function measurements. *Geophysical Journal International*, *184*, 1223–1236.
Rudolph, M. R., Lekic, V., & Lithgow-Bertelloni, C. (2015). Viscosity jump in Earth's mid-mantle. *Science*, *350*, 1349–1352.
Simmons, N. A., Forte, A. M., Boschi, L., & Grand, S. (2010). GyPSuM: A joint tomographic model of mantle density and seismic wave speeds. *Journal of Geophysical Research*, *115*, B12310. https://doi.org/10.1029/2010JB007631
Simmons, N. A., Forte, A. M., & Grand, S. P. (2007). Thermochemical structure and dynamics of the African superplume. *Geophysical Research Letters*, *34*, L02301. https://doi.org/10.1029/2006GL028009
Simmons, N. A., Myers, S. C., Johannesson, G., Matzel, E., & Grand, S. P. (2015). Evidence for long-lived subduction of an ancient tectonic plate beneath the southern Indian Ocean. *Geophysical Research Letters*, *42*, 9270–9278. https://doi.org/10.1002/2015GL066237
Spasojevic, S., Gurnis, M., & Sutherland, R. (2010). Mantle upwellings above slab graveyards linked to the global geoid lows. *Nature Geoscience*, *3*, 435–438.
Steinberger, B. (2000). Slabs in the lower mantle–Results of dynamic modelling compared with tomographic images and the geoid. *Physics of the Earth and Planetary Interiors*, *118*, 241–257.
Steinberger, B., & Calderwood, A. (2006). Models of large-scale viscous flow in the Earth's mantle with constraints from mineral physics and surface observations. *Geophysical Journal International*, *167*, 1461–1481. https://doi.org/10.1111/j.1365-246X.2006.03131.x
Steinberger, B., & Holme, R. (2008). Mantle flow models with core-mantle boundary constraints and chemical heterogeneities in the lowermost mantle. *Journal of Geophysical Research*, *113*, B05403. https://doi.org/10.1029/2007JB005080
Steinberger, B., Seidel, M. L., & Torsvik, T. H. (2017). Limited true polar wander as evidence that Earth's nonhydrostatic shape is persistently triaxial. *Geophysical Research Letters*, *44*, 827–834. https://doi.org/10.1002/2016GL071937
Steinberger, B., & Torsvik, T. H. (2012). A geodynamic model of plumes from the margins of Large Low Shear Velocity Provinces. *Geochemistry, Geophysics, Geosystems*, *13*, Q01W09. https://doi.org/10.1029/2011GC003808
Steinberger, B., Torsvik, T. H., & Becker, T. W. (2012). Subduction to the lower mantle—A comparison between geodynamic and tomographic models. *Solid Earth*, *3*, 415–432.
Tosi, N., Cadek, O., & Martinec, Z. (2009). Subducted slabs and lateral viscosity variations: Effects on the long wavelength geoid. *Geophysical Journal International*, *179*, 813–826.
Wang, X., Holt, W. E., & Ghosh, A. (2015). Joint modeling of lithosphere and mantle dynamics: Evaluation of constraints from global tomography models. *Journal of Geophysical Research: Solid Earth*, *120*, 8633–8655. https://doi.org/10.1002/2015JB012188
Wen, L., & Anderson, D. L. (1997). Layered mantle convection: A model for geoid and topography. *Earth and Planetary Science Letters*, *146*, 367–377.
Yoshida, M., & Nakakuki, T. (2009). Effects on the long-wavelength geoid anomaly of lateral viscosity variations caused by stiff subducting slabs, weak plate margins and lower mantle rheology. *Physics of the Earth and Planetary Interiors*, *172*, 278–288.
Zhong, S. (2001). Role of ocean-continent contrast and continental keels on plate motion, net rotation of lithosphere and the geoid. *Journal of Geophysical Research*, *106*, 703–712.
Zhong, S., & Davies, G. (1999). Effects of plate and slab viscosities on the geoid. *Earth and Planetary Science Letters*, *170*, 487–496.
Zhong, S., McNamara, A. K., Tan, E., Moresi, L. N., & Gurnis, M. (2008). A benchmark study on mantle convection in a 3-D spherical shell using CitcomS. *Geochemistry, Geophysics, Geosystems*, *9*, Q10017. https://doi.org/10.1029/2008GC002048
Zhong, S., Zuber, M. T., Moresi, L. N., & Gurnis, M. (2000). The role of temperature-dependent viscosity and surface plates in spherical shell models of mantle convection. *Journal of Geophysical Research*, *105*, 11,063–11,082.